# Quantum field theoretical structure of electrical conductivity of cold and dense fermionic matter in the presence of a magnetic field

Sarthak Satapathy,[1,2,†] Snigdha Ghosh[3,*] and Sabyasachi Ghosh[1,‡]

[1]*Indian Institute of Technology Bhilai, GEC Campus, Sejbahar, Raipur 492015, Chhattisgarh, India*
[2]*School of Physical Sciences, National Institute of Science Education and Research,*
*Bhubaneswar, HBNI, Jatni 752050, India*
[3]*Government General Degree College Kharagpur-II, Paschim Medinipur 721149, West Bengal, India*

We have gone through a detailed calculation of the two-point correlation function of vector currents at finite density and magnetic field by employing the real time formalism of finite temperature field theory and Schwinger's proper-time formalism. With respect to the direction of the external magnetic field, the parallel and perpendicular components of electric conductivity for the degenerate relativistic fermionic matter are obtained from the zero-momentum limit of the current-current correlator, using the Kubo formula. Our quantum-field theoretical expressions and numerical estimations are compared with those obtained from the relaxation-time approximation methods of kinetic theory and its Landau quantized extension, which can be called classical and quantum results, respectively. All the results are merged in the classical domain i.e., the high-density and low-density magnetic field region, but in the remaining (quantum) domain, quantum results carry a quantized information like the Shubnikov-de Haas oscillation along the density and magnetic field axes. We have obtained a completely new quantum-field theoretical expression for perpendicular conductivity of degenerate relativistic fermionic matter. Interestingly, our quantum field theoretical calculation provides a new mathematical form of the cyclotron frequency with respect to its classical definition, which might require more future research to interpret the phenomena.

## I. INTRODUCTION

An extremely high density and strong magnetic field [1] is naturally found in compact stars like white dwarf (WD) and neutron stars (NS), which have long been studied as a focus research problem of the nuclear and astrophysics sector. These happen to be the dead remnants of massive stars, the cores of which have collapsed during supernovae collision and a complicated layer structure has formed leading to a compact structure as the leftover; they are not massive enough to form black holes because of an incomplete collapse. Based on various studies [2,3], we know a gross range from $10^{12}$ G [2] to $10^{15}$ G [3] for the surface magnetic fields in NS. With increasing depth the density of matter increases reaching up to $\rho = 2.8 \times 10^{14}$ gm/cm$^3$ [4]. At this density nucleons cease to exist and the matter is made up of quarks. From Maxwell's equations, we know that magnetic flux is conserved. This leads to the conclusion that the strength of the magnetic field is $>10^{16}$ G in the interior of neutron stars and magnetars. The strength of the magnetic field varies depending on the nature of the core. For a core made up of neutrons the magnetic field produced is of the order $10^{18}$ G and for a quark core [5] it is of the order of $10^{20}$ G [6]. This magnetic field strength of NS can have ohmic decay profile, which depends on the electrical conductivity of the NS [7]. To solve the relativistic magnetohydrodynamics equations for simulating magnetized neutron stars or binary star mergers, the electrical conductivity of the crustal matter becomes an important input [8–12]. Due to the recently observed gravitational wave signal GW170817 [13], the binary-neutron star merger simulation has gained attention, thus unfolding a new field of research—multimessenger astronomy. In these connections, the microscopic calculation of electrical conductivity in presence of a magnetic field might be an important research topic. One can find a long history with a long list of references (e.g., Refs. [14–17]) for the microscopic calculation of electrical conductivity for compact star but those references have not considered the impact of the magnetic field. For those calculations at a finite magnetic

*Corresponding author.
snigdha.physics@gmail.com
†sarthaks@iitbhilai.ac.in
‡sabyaphy@gmail.com

field picture, the reader can go through the Refs. [18–24], among which Refs. [20,22] have only explored the quantum effect or Landau quantization aspect in the electrical conductivity expressions.

A similar kind of microscopic calculations [25–38] in high-temperature and low-density QCD matter, can be produced in heavy ion collision (HIC) experiments like relativistic heavy ion collision (RHIC) and large hadron collider (LHC). By increasing the temperature, one can expect the hadron to quark phase transition to occur at nearly zero (net) quark/baryon density. This early Universe environment can be expected in RHIC or LHC experiments, where a huge magnetic field can also be created in the peripheral collisions. One can expect a super-hot massless quark gluon plasma (QGP) under a strong magnetic field, whose conductivity expression for classical, quantum field theory cases are respectively discussed in Refs. [34,39]. Here, classical terminology is used for the case, where no Landau quantizations have not been considered and calculations are based on the relaxation time approximation (RTA) based kinetic theory. One can impose Landau quantizations into RTA expressions to get their quantum expressions [37], but they are not same exactly as Kubo expressions [39], which can be considered as quantum field theoretical expressions. Similar to the super-hot massless QGP at strong magnetic field in RHIC or LHC experiments, the core of the NS [5,40] can have a super-dense massless quark matter with a strong magnetic field, whose classical to quantum estimation has been done in Ref. [41]. In the present work, we will explore its quantum field theoretical structure. Previously in Ref. [39], we explored the same field theoretical structure in the high-temperature and magnetic-field domain. Interestingly, the field theoretical structure in the high-temperature and magnetic-field domain, which is addressed in present work, is showing an oscillatory pattern along the magnetic field or density axis. This kind of oscillatory pattern in the condensed matter field is well-known fact in the low-temperature and strong-magnetic field domain and it is popularly called Shubnikov–de Haas (SdH) effect [42–45] or SdH oscillations where it was found that the resistivity oscillates as a function of the magnetic field. The SdH effect is a purely quantum mechanical effect. A similar kind of quantized effect probably can be noticed in quark core of NS, facing a strong magnetic field. This possibility is indicated by Ref. [41] via RTA methods with Landau quantization, while the present article reveals the same possibility via quantum field theoretical methods, carrying some enriched structure. With the help of Schwinger's proper-time methods [46–55] and the real time formalism (RTF) of thermal field theory [56–62], we have calculated the vector current-current correlation function involving fermionic fields, whose zero-momentum limit, based on Kubo-Zubarev formalism [63–66], provides a rich field theoretical expression of conductivity.

The article is organized as follows. In Sec. II, we have addressed the detail calculation of two-point function at finite density and magnetic field, which at the end reaches the final expressions of parallel and perpendicular conductivity components of degenerate quark matter. In Sec. III, we have generated our quantum field theoretical resuluts, which are compared with the classical and quantum results, defined in an earlier work. In Sec. IV summarizes our studies and zoom in the field theoretical ingredients, which is addressed for first time here. Some anatomy of the calculations are presented in the Appendix.

We use natural units in which $\hbar = c = k_B = 1$. The metric tensor has signature $g^{\mu\nu} = \text{diag}(1, -1, -1, -1)$. With respect to the $\hat{z}$-direction, we decompose any four vector $k^\mu$ as $k = (k_\parallel + k_\perp)$, where $k_\parallel^\mu = g_\parallel^{\mu\nu} k_\nu$ and $k_\perp^\mu = g_\perp^{\mu\nu} k_\nu$ in which the corresponding decomposition of the metric tensor is $g^{\mu\nu} = (g_\parallel^{\mu\nu} + g_\perp^{\mu\nu})$ with $g_\parallel^{\mu\nu} = \text{diag}(1,0,0,-1)$ and $g_\perp^{\mu\nu} = \text{diag}(0,-1,-1,0)$. Note that, $k_\perp^2 = -(k_x^2 + k_y^2) < 0$ is a spacelike vector.

## II. FORMALISM

Let us consider a system of noninteracting charged fermions of mass $m$ and charge $e > 0$ in a constant background magnetic field $\boldsymbol{B} = B\hat{z}$. The system is described by the Lagrangian (density),

$$\mathcal{L}_{\text{Dirac}} = \bar{\psi}[i\gamma^\mu D_\mu - m]\psi, \tag{1}$$

where $\psi, \bar{\psi}$ are the conjugate Dirac fields, $D_\mu = \partial_\mu + ie\tilde{A}_\mu$ is the gauge-covariant derivative owing to the minimal electromagnetic coupling, and, $\tilde{A}^\mu = A^\mu + A_{\text{ext}}^\mu$. Here, $A^\mu$ is the dynamical photon field and $A_{\text{ext}}^\mu$ is the classical four-potential arising from the background magnetic field. The calculation will be valid even if the fermion field $\psi$ is a multiplet.

To calculate the electrical conductivity ($\sigma$), we first require the in-medium thermodense magnetic-spectral function $\rho^{\mu\nu}(q)$, calculated from the ensemble average of the two-point correlation function of local vector currents, given by [39]

$$\rho^{\mu\nu}(q) = \tanh\left(\frac{q^0}{2T}\right)\text{Im}\, i \int d^4 x\, e^{iq \cdot x}\langle \mathcal{T}_C J^\mu(x) J^\nu(0)\rangle_{11}^B, \tag{2}$$

where $J^\mu(x)$ denotes the conserved Noether's current corresponding to the $U(1)$ global gauge symmetry of the Lagrangian in Eq. (1), $\mathcal{T}_C$ is the time ordering with respect to the symmetric Schwinger-Keldysh contour $C$ in the complex time plane (shown in Fig. 1) as used in the RTF of finite-temperature field theory [53,56–61], and, the subscript '11' refers to the fact that the two points are on the real horizontal segment of $C$. The explicit form of the current $J^\mu(x)$ reads
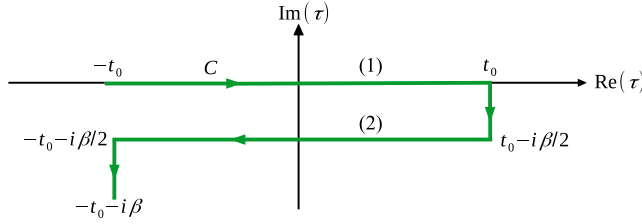
FIG. 1. The symmetric Schwinger-Keldysh contour $C$ in the complex time $(\tau)$ plane used in the RTF with $t_0 \to \infty$ and inverse temperature $\beta = 1/T$. The two horizontal segments of the contour are labeled as '(1)' and '(2)', respectively.

$$J^\mu(x) = e\bar{\psi}\gamma^\mu\psi. \qquad (3)$$

Using Eq. (3), we now calculate the two-point correlation function $\langle \mathcal{T}_C J^\mu(x)J^\nu(0)\rangle^B_{11}$, the details of which are provided in Appendix A. From Eq. (A8), we read off the final result as

$$\langle \mathcal{T}_C J^\mu(x)J^\nu(0)\rangle^B_{11} = -\sum_{l=0}^{\infty}\sum_{n=0}^{\infty}\iint \frac{d^4p}{(2\pi)^4}\frac{d^4k}{(2\pi)^4}e^{-ix\cdot(p-k)}$$
$$\times D_{11}(p_\parallel, m_n)D_{11}(k_\parallel, m_l)\mathcal{N}^{\mu\nu}_{ln}(k,p), \qquad (4)$$

where $m_l = \sqrt{m^2 + 2leB}$ is the effective Landau level dependent mass, and, $D_{11}$ and $\mathcal{N}^{\mu\nu}_{ln}$ are defined respectively in Eqs. (A6) and (A10). On substituting Eq. (4) into Eq. (2) and simplifying, we obtain (after a bit of algebra),

$$\rho^{\mu\nu}(q) = -\tanh\left(\frac{q^0}{2T}\right)\text{Im}\, i\int \frac{d^4k}{(2\pi)^4}\sum_{n=0}^{\infty}\sum_{l=0}^{\infty}D_{11}(k_\parallel, m_l)$$
$$\times D_{11}(p_\parallel = q_\parallel + k_\parallel, m_n)\mathcal{N}^{\mu\nu}_{ln}(k, p = q+k). \quad (5)$$

Again substituting the expression of $D_{11}$ from Eq. (A6) into Eq. (5) and performing the $dk_0 d^2k_\perp$ integral, we get

$$\rho^{\mu\nu}(q) = \tanh\left(\frac{q^0}{2T}\right)\pi\sum_{l=0}^{\infty}\sum_{n=0}^{\infty}\int_{-\infty}^{\infty}\frac{dk_z}{2\pi}\frac{1}{4\omega_{kl}\omega_{pn}}$$

$$\times [\{1 - f_-(\omega_{kl}) - f_+(\omega_{pn}) + 2f_-(\omega_{kl})f_+(\omega_{pn})\}\tilde{\mathcal{N}}^{\mu\nu}_{ln}(k_0 = -\omega_{kl})\delta(q_0 - \omega_{kl} - \omega_{pn})$$

$$+ \{1 - f_+(\omega_{kl}) - f_-(\omega_{pn}) + 2f_+(\omega_{kl})f_-(\omega_{pn})\}\tilde{\mathcal{N}}^{\mu\nu}_{ln}(k_0 = \omega_{kl})\delta(q_0 + \omega_{kl} + \omega_{pn})$$

$$+ \{-f_-(\omega_{kl}) - f_-(\omega_{pn}) + 2f_-(\omega_{kl})f_-(\omega_{pn})\}\tilde{\mathcal{N}}^{\mu\nu}_{ln}(k_0 = -\omega_{kl})\delta(q_0 - \omega_{kl} + \omega_{pn})$$

$$+ \{-f_+(\omega_{kl}) - f_+(\omega_{pn}) + 2f_+(\omega_{kl})f_+(\omega_{pn})\}\tilde{\mathcal{N}}^{\mu\nu}_{ln}(k_0 = \omega_{kl})\delta(q_0 + \omega_{kl} - \omega_{pn})], \qquad (6)$$

where $\omega_{kl} = \sqrt{k_z^2 + m_l^2}$, $\omega_{pn} = \sqrt{(p_z + q_z)^2 + m_n^2}$, $f_\pm(\omega) = [e^{(\omega \mp \mu)/T} + 1]^{-1}$ are the Fermi-Dirac thermal distribution functions, and, $\tilde{\mathcal{N}}^{\mu\nu}_{ln}(k_\parallel) = \int \frac{d^2k_\perp}{(2\pi)^2}\mathcal{N}^{\mu\nu}_{ln}(k,k)$ can be read off from Eq. (A19) as

$$\tilde{\mathcal{N}}^{\mu\nu}_{ln}(k_\parallel) = e^2\frac{eB}{\pi}[-4eBn\delta^{n-1}_{l-1}g^{\mu\nu}_\parallel - (\delta^n_l + \delta^{n-1}_{l-1})\{2k^\mu_\parallel k^\nu_\parallel - g^{\mu\nu}_\parallel(k^2_\parallel - m^2)\} + (\delta^{n-1}_l + \delta^n_{l-1})(k^2_\parallel - m^2)g^{\mu\nu}_\perp]. \qquad (7)$$

The right-hand side of Eq. (6) contains four Dirac delta functions and they give rise to the branch cuts of the spectral function in the complex energy $(q^0)$ plane. The first two delta functions are called the unitary cuts whereas the last two delta functions are termed as the Landau cuts. In order to calculate transport coefficients, we need to take the static (long-wavelength) limit i.e., $\mathbf{q} = 0, q^0 \to 0$ of the spectral function in Eq. (6), so that only the Landau cuts contribute and we are left with

$$\rho^{\mu\nu}(q_0, \mathbf{q} = \mathbf{0}) = \tanh\left(\frac{q^0}{2T}\right)\pi\sum_{l=0}^{\infty}\sum_{n=0}^{\infty}\int_{-\infty}^{\infty}\frac{dk_z}{2\pi}\frac{1}{4\omega_{kl}\omega_{kn}}$$

$$\times \left[\{-f_-(\omega_{kl}) - f_-(\omega_{kn}) + 2f_-(\omega_{kl})f_-(\omega_{kn})\}\tilde{\mathcal{N}}^{\mu\nu}_{ln}(k_0 = -\omega_{kl})\delta(q_0 - \omega_{kl} + \omega_{kn})\right.$$

$$\left. + \{-f_+(\omega_{kl}) - f_+(\omega_{kn}) + 2f_+(\omega_{kl})f_+(\omega_{kn})\}\tilde{\mathcal{N}}^{\mu\nu}_{ln}(k_0 = \omega_{kl})\delta(q_0 + \omega_{kl} - \omega_{kn})\right]$$

$$= \lim_{\Gamma \to 0}\tanh\left(\frac{q^0}{2T}\right)\sum_{l=0}^{\infty}\sum_{n=0}^{\infty}\int_{-\infty}^{\infty}\frac{dk_z}{2\pi}\frac{1}{4\omega_{kl}\omega_{kn}}$$

$$\times \left[\{-f_-(\omega_{kl}) - f_-(\omega_{kn}) + 2f_-(\omega_{kl})f_-(\omega_{kn})\}\tilde{\mathcal{N}}^{\mu\nu}_{ln}(k_0 = -\omega_{kl})\frac{\Gamma}{\Gamma^2 + (q_0 - \omega_{kl} + \omega_{kn})^2}\right.$$

$$\left. + \{-f_+(\omega_{kl}) - f_+(\omega_{kn}) + 2f_+(\omega_{kl})f_+(\omega_{kn})\}\tilde{\mathcal{N}}^{\mu\nu}_{ln}(k_0 = \omega_{kl})\frac{\Gamma}{\Gamma^2 + (q_0 + \omega_{kl} - \omega_{kn})^2}\right], \qquad (8)$$

where in the last step, we have used the Breit-Wigner representation of the Dirac delta function $\delta(x) = \frac{1}{\pi}\lim_{\Gamma\to 0}\text{Im}(\frac{1}{x-i\Gamma}) = \lim_{\Gamma\to 0}(\frac{\Gamma}{\Gamma^2+x^2})$. The conductivity tensor $\sigma^{\mu\nu}$ in the presence of external magnetic field is obtained in the Kubo formalism by taking the zero-momentum limit of $\rho^{\mu\nu}/q^0$, or alternatively by using L'Hôpital's rule as

$$
\begin{aligned}
\sigma^{\mu\nu}(T,\mu,B) = \frac{\partial\rho^{\mu\nu}}{\partial q_0}\bigg|_{q=0,q_0\to 0} &= \lim_{\Gamma\to 0}\sum_{l=0}^{\infty}\sum_{n=0}^{\infty}\frac{1}{2T}\int_{-\infty}^{\infty}\frac{dk_z}{2\pi}\frac{1}{4\omega_{kl}\omega_{kn}}\frac{\Gamma}{\Gamma^2+(\omega_{kl}-\omega_{kn})^2} \\
&\times [\{-f_-(\omega_{kl}) - f_-(\omega_{kn}) + 2f_-(\omega_{kl})f_-(\omega_{kn})\}\tilde{\mathcal{N}}_{ln}^{\mu\nu}(k_0 = -\omega_{kl}) \\
&+ \{-f_+(\omega_{kl}) - f_+(\omega_{kn}) + 2f_+(\omega_{kl})f_+(\omega_{kn})\}\tilde{\mathcal{N}}_{ln}^{\mu\nu}(k_0 = \omega_{kl})].
\end{aligned}
\tag{9}
$$

Since our focal zone is the core of NS, where an extreme relativistic degenerate (super-dense massless) fermionic matter can be expected, we will impose the $T \to 0$ limit to Eq. (9). In order to take $T \to 0$ limit to Eq. (9), we first rewrite it as

$$
\begin{aligned}
\sigma^{\mu\nu}(T,\mu,B) = -\lim_{\Gamma\to 0}\sum_{l=0}^{\infty}\sum_{n=0}^{\infty}\frac{1}{2}\int_{-\infty}^{\infty}\frac{dk_z}{2\pi}&\frac{1}{4\omega_{kl}\omega_{kn}}\frac{\Gamma}{\Gamma^2+(\omega_{kl}-\omega_{kn})^2} \\
\times \bigg[&\bigg\{\frac{f_-(\omega_{kl})}{f_-(\omega_{kn})}\frac{\partial}{\partial\mu}f_-(\omega_{kn}) + \frac{f_-(\omega_{kn})}{f_-(\omega_{kl})}\frac{\partial}{\partial\mu}f_-(\omega_{kl})\bigg\}\tilde{\mathcal{N}}_{ln}^{\mu\nu}(k_0 = -\omega_{kl}) \\
&+ \bigg\{\frac{f_+(\omega_{kl})}{f_+(\omega_{kn})}\frac{\partial}{\partial\mu}f_+(\omega_{kn}) + \frac{f_+(\omega_{kn})}{f_+(\omega_{kl})}\frac{\partial}{\partial\mu}f_+(\omega_{kl})\bigg\}\tilde{\mathcal{N}}_{ln}^{\mu\nu}(k_0 = \omega_{kl})\bigg].
\end{aligned}
\tag{10}
$$

In the zero-temperature limit, the thermal distribution function will behave like the Heaviside step function $\Theta(x)$ as

$$
\lim_{T\to 0}f_\pm(\omega) = \lim_{T\to 0}\frac{1}{e^{(\omega\mp\mu)/T}+1} = \Theta(-\omega\pm\mu). \tag{11}
$$

where, the step function is defined as

$$
\Theta(x) = \begin{cases} 1 & \text{if } x > 0, \\ 1/2 & \text{if } x = 0, \\ 0 & \text{if } x < 0. \end{cases} \tag{12}
$$

Using Eqs. (11) and (12) in Eq. (10), we get after some simplifications

$$
\begin{aligned}
\sigma^{\mu\nu}(T\to 0,\mu,B) = -\lim_{\Gamma\to 0}\sum_{l=0}^{\infty}\sum_{n=0}^{\infty}\int_{-\infty}^{\infty}\frac{dk_z}{2\pi}&\frac{1}{4\omega_{kl}\omega_{kn}}\frac{\Gamma}{\Gamma^2+(\omega_{kl}-\omega_{kn})^2} \\
\times [&\{\Theta(-\mu-\omega_{kl})\delta(-\mu-\omega_{kn}) + \Theta(-\mu-\omega_{kn})\delta(-\mu-\omega_{kl})\}\tilde{\mathcal{N}}_{ln}^{\mu\nu}(k_0 = -\omega_{kl}) \\
&+ \{\Theta(\mu-\omega_{kl})\delta(\mu-\omega_{kn}) + \Theta(\mu-\omega_{kn})\delta(\mu-\omega_{kl})\}\tilde{\mathcal{N}}_{ln}^{\mu\nu}(k_0 = \omega_{kl})].
\end{aligned}
\tag{13}
$$

Finally considering the fermion chemical potential $\mu > 0$, the antiparticle distributions will not contribute to the spectral function. Even at low $T$ and high density region, one can safely discard the subleading antiparticle contribution to the spectral functions. Thus, ignoring the antiparticle part in Eq. (13), we get

$$
\begin{aligned}
\sigma^{\mu\nu}(T\to 0,\mu>0,B) = -\lim_{\Gamma\to 0}\sum_{l=0}^{\infty}\sum_{n=0}^{\infty}\int_{-\infty}^{\infty}\frac{dk_z}{2\pi}&\frac{1}{4\omega_{kl}\omega_{kn}}\frac{\Gamma}{\Gamma^2+(\omega_{kl}-\omega_{kn})^2}\tilde{\mathcal{N}}_{ln}^{\mu\nu}(k_0 = \omega_{kl}) \\
&\times \{\Theta(\mu-\omega_{kl})\delta(\mu-\omega_{kn}) + \Theta(\mu-\omega_{kn})\delta(\mu-\omega_{kl})\}.
\end{aligned}
\tag{14}
$$

In the presence of background magnetic field, all the transport coefficients including the electrical conductivity $\sigma^{\mu\nu}$ become anisotropic. The electrical conductivity parallel ($\parallel$) and perpendicular ($\perp$) to the magnetic-field direction can be calculated from

$$
\sigma_\parallel = b^\alpha b^\beta \Delta_{\alpha\mu}\Delta_{\beta\nu}\sigma^{\mu\nu}, \tag{15}
$$

$$
\sigma_\perp = -\frac{1}{2}\Xi^{\alpha\beta}\Delta_{\alpha\mu}\Delta_{\beta\nu}\sigma^{\mu\nu}, \tag{16}
$$

where, $\Delta^{\mu\nu} = (g^{\mu\nu} - u^\mu u^\nu)$ is a projector orthogonal to $u^\mu$, $b^\mu = \frac{1}{2B}\varepsilon^{\mu\nu\alpha\beta}F_{\nu\alpha}u_\beta$, $F_{\mu\nu} = (\partial_\mu A_\nu^{\text{ext}} - \partial_\nu A_\mu^{\text{ext}})$ is the electromagnetic field strength tensor, and, $\Xi^{\mu\nu} = (\Delta^{\mu\nu} + b^\mu b^\nu)$. Here, $u^\mu$ is the medium four-velocity. In the local rest frame (LRF) of the medium $u_{\text{LRF}}^\mu \equiv (1,\mathbf{0})$ and $b_{\text{LRF}}^\mu \equiv (0,\hat{z})$. It can be noticed that Eqs. (15) and (16) also yield the following expressions of the parallel and perpendicular conductivities in terms of different components of the conductivity tensor,

$$\sigma_\parallel = \sigma^{33}, \tag{17}$$

$$\sigma_\perp = \frac{1}{2}(\sigma^{11} + \sigma^{22}), \tag{18}$$

which are easier to understand in terms of a physical interpretation.

Until now, $\Gamma$ in Eq. (14) is an infinitesimal parameter corresponding to the Breit-Wigner representation of the Dirac delta function. Since, we have taken a system of noninteracting particles, the transport coefficients should diverge (like the case of an ideal gas) and is apparent from Eq. (14) in the limit $\Gamma \to 0$. In order to get nondivergent values of the electrical conductivity, we must consider finite value of $\Gamma > 0$ which corresponds to switching on the interactions among the particles, thus allowing dissipation in the medium. $\Gamma$ can be identified as the thermal width (or the inverse of relaxation time $\tau_c$). The thermal width $\Gamma$ can be calculated microscopically from the interaction Lagrangian which involves the estimations of the scattering cross sections (decay rates) among (of) the constituent particles in the presence of a magnetic field [67–72]. In present work, we will keep $\Gamma$ as an input parameter and take it of order of QCD scale $\Gamma \approx 10^2$ MeV or its inverse time scale (the relaxation time) $\tau_c \approx 1$ fm. Here our focal interest will be to see the general structure of magnetothermodynamical phase space in electrical conduction for any degenerate and massless Dirac fluid. In the rest of the calculation, we thus continue with a finite value of $\Gamma$. Substituting Eq. (14) into Eqs. (15) and (16), we get

$$\begin{aligned}\sigma_{\parallel,\perp}(\mu,B) = &-\sum_{l=0}^\infty \sum_{n=0}^\infty \int_{-\infty}^\infty \frac{dk_z}{2\pi} \frac{1}{4\omega_{kl}\omega_{kn}} \frac{\Gamma}{\Gamma^2 + (\omega_{kl}-\omega_{kn})^2}\\ &\times \tilde{\mathcal{N}}_{ln}^{\parallel,\perp} \{\Theta(\mu-\omega_{kl})\delta(\mu-\omega_{kn})\\ &+ \Theta(\mu-\omega_{kn})\delta(\mu-\omega_{kl})\},\end{aligned} \tag{19}$$

where

$$\tilde{\mathcal{N}}_{ln}^\parallel = b^\alpha b^\beta \Delta_{\alpha\mu}\Delta_{\beta\nu}\tilde{\mathcal{N}}_{ln}^{\mu\nu}(k_0 = \omega_{kl}), \tag{20}$$

$$\tilde{\mathcal{N}}_{ln}^\perp = -\frac{1}{2}\Xi^{\alpha\beta}\Delta_{\alpha\mu}\Delta_{\beta\nu}\tilde{\mathcal{N}}_{ln}^{\mu\nu}(k_0 = \omega_{kl}). \tag{21}$$

Substituting Eq. (7) into Eqs. (20) and (21) and simplifying, we get

$$\tilde{\mathcal{N}}_{ln}^\parallel = -2e^2 \frac{eB}{\pi} k_z^2(2-\delta_l^0)\delta_l^n, \tag{22}$$

$$\tilde{\mathcal{N}}_{ln}^\perp = -2e^2 \frac{(eB)^2}{\pi} l(\delta_l^{n-1} + \delta_{l-1}^n). \tag{23}$$

Finally substituting Eqs. (22) and (23) into (19) and performing the remaining $dk_z$ integral using the Dirac delta function, we get after some long but straightforward algebra, the following analytic expressions of the parallel and perpendicular conductivities,

$$\sigma_\parallel = e^2\left(\frac{eB}{2\pi^2}\right)\frac{1}{\Gamma\mu}\sum_{l=0}^{l_{\max}}(2-\delta_l^0)\sqrt{\mu^2-m_l^2}\,\Theta(\mu-m_l), \tag{24}$$

$$\begin{aligned}\sigma_\perp = &e^2\left(\frac{eB}{2\pi^2}\right)\frac{\Gamma}{\Gamma^2 + (\mu-\sqrt{\mu^2-2eB})^2}\frac{1}{\sqrt{\mu^2-2eB}}\\ &\times \sum_{l=1}^{l_{\max}}\frac{(2l-1)eB}{\sqrt{\mu^2-m_l^2}}\Theta(\mu-m_l),\end{aligned} \tag{25}$$

where

$$l_{\max} = \left\lfloor \frac{\mu^2-m^2}{2eB} \right\rfloor, \tag{26}$$

in which the floor function $\lfloor x \rfloor =$ 'largest integer less than or equal to $x$'. It can be observed that the presence of the Kronecker delta functions in Eqs. (22) and (23) have killed one of the double sums of Eq. (19) and the presence of the step functions $\Theta(\mu-m_l)$ in Eqs. (24) and (25) have restricted the upper limit of the infinite sum over index $l$ to $l_{\max}$ given in Eq. (26). The step function $\Theta(\mu-m_l)$ also ensures that $\mu$ has to be greater than $2eB$ for a non-vanishing $\sigma_\perp$.

It is also worth noticing that, the presence of the Dirac delta functions in Eq. (14) have made the Fermi-momentum along the $\hat{z}$ direction $k_{zl}^F$ to be quantized as

$$\begin{aligned}k_{zl}^F = &\pm\sqrt{\mu^2-m^2-2leB}; \qquad l \in \{0,\mathbb{Z}^+\}\\ = &\pm\sqrt{\mu^2-m^2},\pm\sqrt{\mu^2-m^2-2eB},\ldots,\\ &\pm\sqrt{\mu^2-m^2-2l_{\max}eB}.\end{aligned} \tag{27}$$

## III. NUMERICAL RESULTS AND DISCUSSIONS

Lets us start our result section first by a simple graphical representation of maximum value of Landau level $l_{\max}$ as a function of $eB$ and $\mu$ in Figs. 2(a) and 2(b), which will be very useful to understand our latter results. We have plotted integers values of $l_{\max} = \lfloor \frac{\mu^2-m^2}{2eB} \rfloor$ vs $eB$ and $\mu$ in Figs. 2(a) and 2(b) for massless fermionic matter at different values of
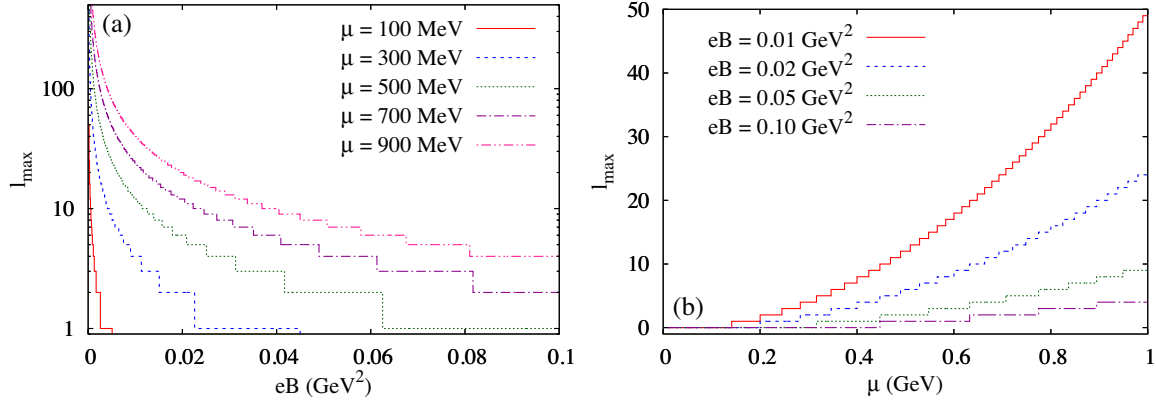
FIG. 2.   The variation of $l_{max}$ as a function of (a) a magnetic field for different values of chemical potential, and (b) the chemical potential for different values of magnetic field.

$\mu$ and $eB$, respectively. Here one can see a rough transition from continuous to quantized pattern as, we increase $eB$ and decrease $\mu$. It may be considered as a visual transition from a classical zone with low $eB$ and/or high $\mu$ to a quantum zone with high $eB$ and/or low $\mu$.

Next, our aim is to have numerical discussions of the field theoretical expressions of conductivity components, given in Eqs. (24) and (25). To understand the field theoretical contribution in these expressions, let us quickly recapitulate the classical and quantum mechanical expressions of conductivity in magnetic fields from Ref. [41]. In the presence of a magnetic field, the electrical conductivity at zero temperature and finite $\mu$ is obtained from the RTA formalism $\sigma_{\parallel,\perp}$ as [41]

$$\sigma_{\parallel,\perp}^{RTA} = 2e^2 \int \frac{d^3k}{(2\pi)^3} \tau_c^{\parallel,\perp} \frac{\vec{k}^2}{3\omega_k^2} \delta(\omega_k - \mu)$$
$$= \frac{e^2}{3\pi^2} \frac{(\mu^2 - m^2)^{3/2}}{\mu} \tau_c^{\parallel,\perp}, \tag{28}$$

where $\omega_k = \sqrt{\vec{k}^2 + m^2}$ is the single particle energy and $\tau_c^{\parallel,\perp}$ are the effective relaxation times given by

$$\tau_c^{\parallel} = \tau_c, \tag{29}$$

$$\tau_c^{\perp} = \frac{\tau_c}{1 + \frac{\tau_c^2}{\tau_B^2}}, \tag{30}$$

in which $\tau_c$ is the relaxation time in the absence of magnetic field and $\tau_B = \frac{\mu}{eB}$ is the inverse of cyclotron frequency. It is noted that the actual definition of $\tau_B$ is given by $\tau_B(\omega_k) = \frac{\omega_k}{eB}$ which becomes $\tau_B = \frac{\mu}{eB}$ in Eq. (28) due to the presence of the Dirac delta function in the integrand. The RTA expression of $\sigma_{\parallel,\perp}$ which may be called the classical mechanical (CM) expressions, gets modified on the imposition of Landau quantization to the energy-momentum relation of charged

particles and we obtain the quantum mechanical (QM) version of $\sigma_{\parallel,\perp}$. The classical to quantum transformation is done by hand to modify the energy-momentum relation $\omega_k = \sqrt{\vec{k}^2 + m^2} \to \omega_{kl} = \sqrt{k_z^2 + m^2 + 2leB}$, where $k_z$ is the momentum along $\hat{z}$-direction (in the direction of magnetic field) and $l$ is the Landau level. The modified QM expressions are given by [41]

$$\sigma_{\parallel}^{QM} = \sum_{l=0}^{\infty} \alpha_l e^2 \frac{eB}{2\pi^2} \int_0^{\infty} dk_z \frac{k_z^2}{\omega_{kl}^2} \tau_c^{\parallel} \delta(\omega_{kl} - \mu)$$
$$= \frac{e^2}{2\pi^2} eB \sum_{l=0}^{l_{max}} \alpha_l \frac{\sqrt{\mu^2 - 2leB - m^2}}{\mu} \tau_c^{\parallel}, \tag{31}$$

$$\sigma_{\perp}^{QM} = \sum_{l=0}^{\infty} \alpha_l e^2 \frac{eB}{2\pi^2} \int_0^{\infty} dk_z \frac{leB}{\omega_{kl}^2} \tau_c^{\perp} \delta(\omega_{kl} - \mu)$$
$$= \frac{e^2}{2\pi^2} eB \sum_{l=1}^{l_{max}} \frac{2leB}{\mu\sqrt{\mu^2 - 2leB - m^2}} \tau_c^{\perp}, \tag{32}$$

where $\alpha_l = (2 - \delta_l^0)$ and the summation has been performed up to the highest Landau level $l_{max} = \lfloor \frac{\mu^2 - m^2}{2eB} \rfloor$. Similar to the RTA expressions $\sigma_{\parallel,\perp}^{RTA}$ and quantum mechanical expressions $\sigma_{\parallel,\perp}^{QM}$, we can call the Kubo expressions of Eqs. (24) and (25) as $\sigma_{\parallel,\perp}^{QFT}$, since the calculations are based on quantum field theory at finite $\mu$ and $B$.

Next, we have generated the curves for conductivity components of RTA, QM, and QFT. In all the graphs, we have considered the variations of the dimensionless quantity $\sigma/(\tau_c\mu^2)$ with $eB$ and $\mu$. We have also fixed $\tau_c = \Gamma^{-1} = 10$ fm for all the results. An interesting part of our results is the oscillatory behavior of the QM and QFT curves, which can be realized as so-called Shubnikov-de Haas (SdH) effect [42–45,53,73,74] or SdH oscillations. In this effect, at low temperatures and at intense magnetic fields, the electrical conductivity can oscillate. This

phenomena is quite well known in condensed matter physics. The present work indicates a possibility of this phenomena in compact star environment, where a strong magnetic field is also expected in dense matter.

It has also been seen that SdH oscillations affect the transport and thermodynamic properties of the material [53]. It was shown in Ref. [53] that the free energy of a compact star exhibits prominent oscillatory modes at low temperatures and vanishing modes at higher temperatures. The results of Ref. [53] is one of the pioneering works where the oscillations were observed to occur in the thermodynamic properties quark matter. The origin of this effect is purely quantum mechanical. In the forthcoming paragraphs, we have explored that quantum effect by comparing the RTA, QM, and QFT curves, where the field theoretical changes are our central attention as the main contribution.

In Figs. 3(a) and 3(b), we have plotted the variation of $\sigma^{\parallel}/(\tau_c\mu^2)$ as a function of $eB$ and $\mu$ for CM/RTA, QM, and QFT estimations. Comparing Eqs. (24) and (31), we see that the QM expression $\sigma_{\parallel}^{\mathrm{QM}}$ exactly matches with the corresponding QFT expression $\sigma_{\parallel}^{\mathrm{QFT}}$. However, the QM expressions are obtained by imposing Landau quantization on to the CM expression by hand, whereas, the QFT expression is obtained from microscopic calculation in terms of the in-medium spectral function. In Fig. 3(a), the red colored solid horizontal line is the RTA curve which is found to be independent of the magnetic field. This is expected in the classical picture as the Lorentz force does not do any work in the direction of magnetic field, but this argument does not work for the QM or QFT picture. We notice a magnetic field dependent parallel conductivity, shown by blue line in Fig. 3(a), which cannot be explained by classical Lorentz force only. Here we see the effect of the Landau quantization of energies which gives rise to the SdH effect leading to an oscillatory graph as shown by Fig. 3(a).

From Fig. 2(a), we already know that lesser number of Landau levels will contribute in conduction as the magnetic field increases. Similarly, for fixed values of $eB$, as we decrease $\mu$, a lesser number of Landau levels will contribute in conduction, which is shown in Fig. 2(b). Hence, the low $\mu$ and large $eB$ domain, where lesser number of Landau levels will contribute, can be consider as quantum domain because the microscopic energy quantization can be revealed in a macroscopic quantity such as the conductivity. An oscillatory conductivity in low $\mu$ and high $eB$ zone is observed because a lesser number of Landau levels will contribute in conduction. The reader can understand this fact from Figs. 3(a) and 3(b). The QM results were also disclosed in Ref. [41]. So, based on present work and the earlier Ref. [41], one can expected the SdH effect or oscillatory pattern in the conductivity of dense quark matter, which may exist in the core of an NS [5].

On the other hand, one can call the low $eB$ and high $\mu$ domain as classical domain since the CM and QM/QFT curves of Figs. 3(a) and 3(b) are merged here. The reader might be misguided by seeing the QM/QFT expressions, given in Eqs. (24) and (31), which are proportional to $eB$ and seemed to be zero in the $eB \to 0$ limit but it is not true. For small values of $eB$, $l_{\max}$ of Eq. (26) will be quite larger and it is through larger no of Landau level summation, conductivity will converge towards a finite values instead of being zero. In the limit $eB \to 0$, the Landau levels will be infinitesimally close to each other and the contributions from an infinite number of such Landau levels add up to the exact continuum result of the CM estimation. From a numerical point of view, reaching $eB = 0$ for QM/QFT curves is quite difficult as for that case an infinite number of Landau levels has to be summed ideally.

Next in Figs. 4(a)–(d), we have shown the variation of $\sigma^{\perp}/(\tau_c\mu^2)$ as a function of $eB$ and $\mu$, respectively. Unlike the CM expression of $\sigma^{\parallel}/(\tau_c\mu^2)$, its perpendicular component has additional $\mu$ and $eB$ dependence due to the factor $1/\{1 + (\frac{\tau_c eB}{\mu})^2\}$ in Eqs. (28) and (30). The factor for small
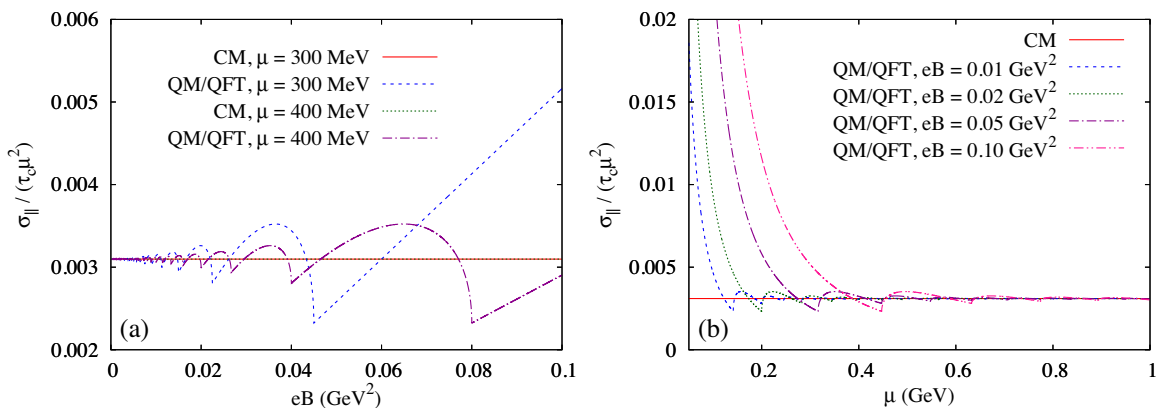


FIG. 3.    The variation of CM and QM/QFT values of $\sigma_{\parallel}/(\tau_c\mu^2)$ as a function of (a) the magnetic field for different values of $\mu$, and (b) fermion chemical potential for different values of $eB$.

values of $eB$ and large values of $\mu$ become close to one. In Figs. 4(c) and 4(d), horizontal black solid line indicates CM curve at $eB = 0$ and the red solid line is the perpendicular component of the CM curves for two different values of $eB$. They are merging at high $\mu$ but the perpendicular component is suppressed from the horizontal line due to the factor. When we generate their QM (dash line) and QFT (dotted line) curves by using Eqs. (32) and (25), we get an oscillatory pattern for both cases. Unlike the parallel component case, the quantitative values of QM and QFT expressions for parallel conductivity are different, which can be understood either by comparing Eqs. (32) and (25) or by minutely noticing the QM (dash line) and QFT (dotted line) curves in Figs. 4(c) and 4(d). This difference is due to the new finding with respect to earlier Ref. [41], where QM estimations are presented. Also, we are probably revealing this new QFT curve in dense sector for the first time, whose difference from QM curve is probably connected with a rich-field theoretical effect. The peaks are due to the divergent term $\frac{1}{\sqrt{\mu^2-m^2-2l_{\max}B}}$ in the expression of $\sigma_\perp^{\text{QM}}$ and $\sigma_\perp^{\text{QFT}}$. These oscillatory curves with a peak pattern will fade as we transit from the quantum domain (low $\mu$ and high $eB$) to the classical domain (high $\mu$ and low $eB$). The merging of CM, QM, and QFT curves at high $\mu$ in Figs. 4(c)

and 4(d) and low $eB$ in Figs. 4(a) and 4(b) is disclosing that fact.

At low $\mu$, the QM and QFT values of perpendicular component can be zero, which is connected with the lowest Landau level (LLL) approximation. Interestingly, the LLL approximation of parallel components will give us nonzero values,

$$\sigma_\parallel^{\text{LLL}} = e^2 \left(\frac{eB}{2\pi^2}\right) \frac{\tau_c}{\mu} \sqrt{\mu^2 - m^2}\, \Theta(\mu - m), \quad \text{so that}$$

$$\frac{\sigma_\parallel^{\text{LLL}}}{\tau_c \mu^2} = \frac{e^2}{2\pi^2} \left(\frac{eB}{\mu^2}\right) \quad \text{for the massless case,} \qquad (33)$$

but the perpendicular component in the LLL approximation become zero, $\sigma_\perp^{\text{LLL}} = 0$. In this extreme low $\mu$ with $\mu^2 \leq 2eB$ or high $eB$ with $eB \geq \mu^2/2$, which might be considered as extreme quantum domain, there will be no conduction in the perpendicular/transverse direction. It means that the 3D anisotropic conduction picture will be transformed to a 1D picture with an extreme anisotropic conduction. We may find a particular domain, where the quark core in NS can reach this LLL or 1D picture.

Due to the oscillating and spikelike nature of $\sigma_\perp$ as shown in Fig. 4, it is difficult to know the actual quantitative
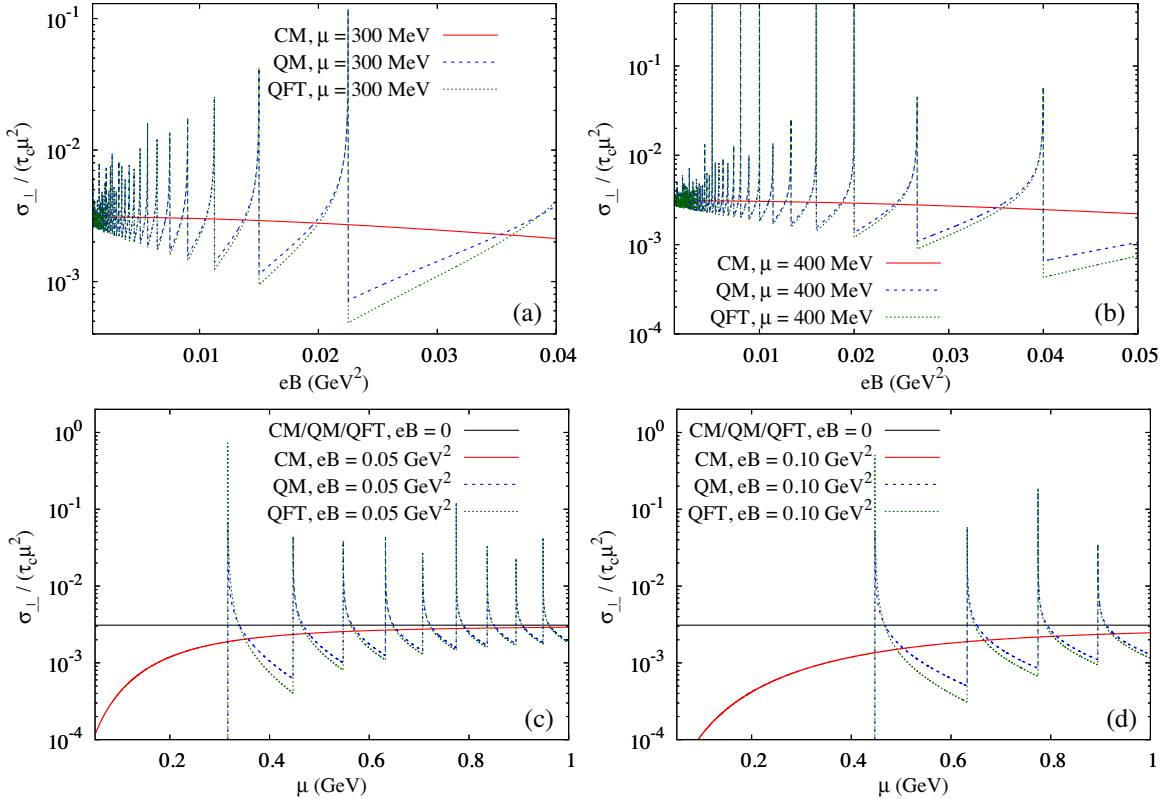


FIG. 4. The variation of the CM, QM, and QFT estimation of $\sigma_\perp/(\tau_c\mu^2)$ as a function of (a) magnetic field for $\mu = 300$ MeV, (b) magnetic field for $\mu = 400$ MeV, (c) fermion chemical potential for $eB = 0.05$ GeV$^2$, and (d) fermion chemical potential for $eB = 0.10$ GeV$^2$. The corresponding $eB = 0$ graphs are also shown in subfigures (c) and (d) for comparison.

difference between the QFT and QM estimations of the perpendicular conductivity component. For this, we have depicted the ratio $\sigma_\perp^{\text{QFT}}/\sigma_\perp^{\text{QM}}$ as a function of the magnetic field and fermion chemical potential in Figs. 5(a) and 5(b), respectively. When $eB$ or $\mu$ values changes, the integer value of $l_{\max} = \lfloor \mu^2/(2eB) \rfloor$ remains the same within a particular interval but when $eB$ or $\mu$ values enter into next possible integer value of $l_{\max}$, then a sudden spike appears at the transition values $eB = \mu^2/(2l_{\max})$ or $\mu = \sqrt{2l_{\max}eB}$. Skipping those spike values at transition $eB$ or $\mu$ points, we can get a gross profile of the ratio $\sigma_\perp^{\text{QFT}}/\sigma_\perp^{\text{QM}}$ along the $eB$ and $\mu$ axes. In the quantum domain (i.e., low $\mu$ and high $eB$ regions), the ratio becomes less than unity but it tends to unity in classical domain (i.e., high $\mu$ and low $eB$ regions) where both the QM and QFT curves merge to the CM curve. Hence, this deviation of ratio from unity signifies that the QFT estimation carries a more enrich quantum effect than the simple Landau quantization concept, embedded in QM estimation. Before entering lowest Landau level (where perpendicular transportation freezes) the ratio receives maximum suppression (around 40%), which is quite strong.

By comparing the CM, QM, and QFT expressions of perpendicular components given in Eqs. (28), (32), and (25) respectively, we want to point out another interesting part of our present investigation. Similar to the classical effective relaxation time $\tau_c^\perp = \tau_c/(1 + \frac{\tau_c^2}{\tau_B^2})$, we can recognize the QFT-based effective relaxation time,

$$\tilde{\tau}_c^\perp = \frac{\Gamma}{\Gamma^2 + (\mu - \sqrt{\mu^2 - 2eB})^2} = \tau_c/\left(1 + \frac{\tau_c^2}{\tilde{\tau}_B^2}\right), \quad (34)$$

where
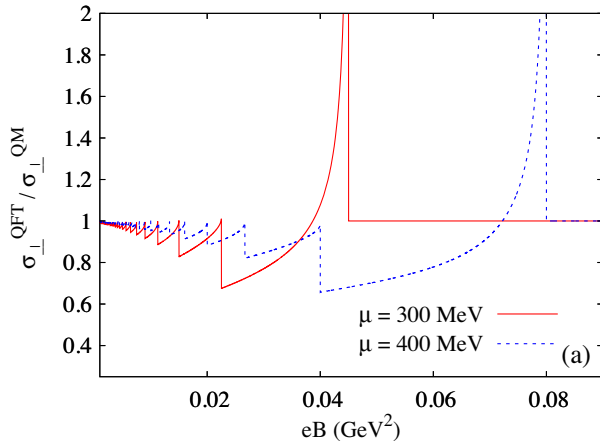
$$\frac{1}{\tilde{\tau}_B} = \left(\mu - \sqrt{\mu^2 - 2eB}\right)$$

$$= \frac{eB}{\mu}\left\{1 + \frac{eB}{2\mu^2} + \frac{(eB)^2}{2\mu^4} + \frac{5(eB)^3}{8\mu^6} + \cdots\right\}$$

$$= \frac{1}{\tau_B}\left\{1 + \frac{1}{2\mu\tau_B} + \frac{1}{2(\mu\tau_B)^2} + \frac{5}{8(\mu\tau_B)^3} + \cdots\right\}. \quad (35)$$

One can see that for $\frac{1}{\mu\tau_B} = \frac{eB}{\mu^2} \to 0$, $\tilde{\tau}_B \to \tau_B$ as expected. So the inverse of cyclotron frequency $\tau_B = \frac{\mu}{eB}$ in the classical domain, i.e., small $eB$ and large $\mu$, will transform into

$$\tilde{\tau}_B = \tau_B/\left\{1 + \frac{1}{2}\left(\frac{eB}{\mu^2}\right) + \frac{1}{2}\left(\frac{eB}{\mu^2}\right)^2 + \frac{5}{8}\left(\frac{eB}{\mu^2}\right)^3 + \cdots\right\}, \quad (36)$$

as we go towards the quantum domain, i.e., large $eB$ and small $\mu$. Interestingly, we can compare this fact with the transition from the nonrelativistic (NR) energy momentum relation $E_{NR} = \frac{p^2}{2m}$ to relativistic (R) series-type relation $E_R = E_{NR}[1 - \frac{1}{4}(\frac{p}{m})^2 + \cdots]$, whose higher-order terms become important as we gradually increase the momentum $p$ or velocity. Similarly, as we increase $eB$ and/or decrease $\mu$ or increase $\frac{eB}{\mu^2}$, higher-order terms of Eq. (36) will be important. So, one may get a comparative feelings between this CM to QFT transition for effective cyclotron frequency and the NR to R transition for kinetic energy. We are addressing this fact for the first time; this probably carries very important field-theoretical information.

In the quantum mechanical expressions, the reader should notice that the classical quantity $\tau_B$ is still present in $\sigma_\perp^{\text{QM}}$, so QM expressions carry a semiclassical picture of particle quantization. Actually, the QM expression is designed by imposing Landau quantization in the CM expression. Therefore, the momentum integration is only modified but other parts remain same as in the CM
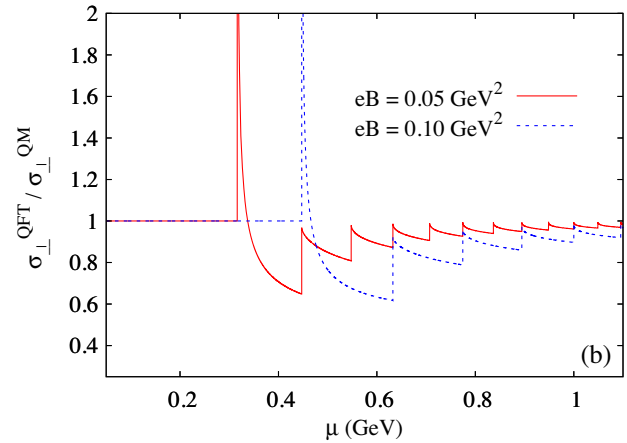


FIG. 5. The variation of $\sigma_\perp^{\text{QFT}}/\sigma_\perp^{\text{QM}}$ as a function of (a) magnetic field for different values of $\mu$, and (b) fermion chemical potential for different values of $eB$.
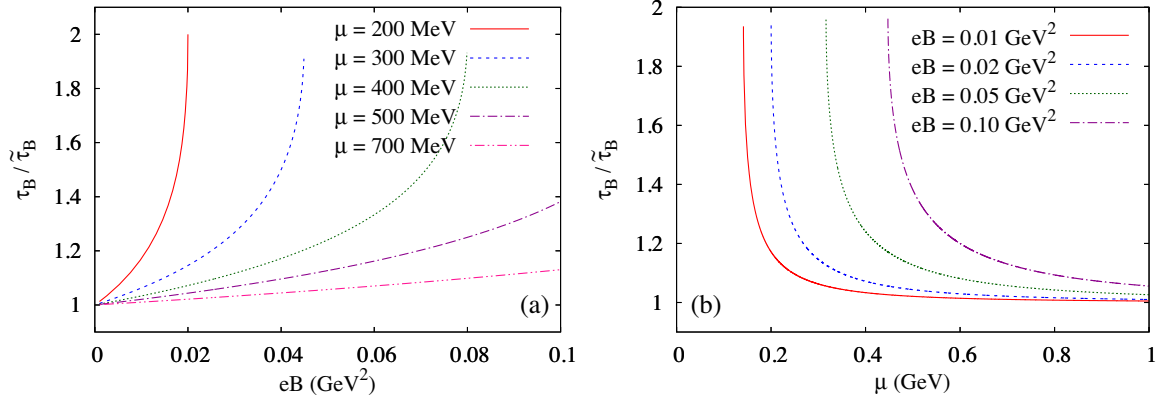
FIG. 6.   The variation of the ratio $\tau_B/\tilde{\tau}_B$ as a function of (a) magnetic field for different values of $\mu$, and (b) fermion chemical potential for different values of $eB$.

expression. A proper quantized picture is found in the field theoretical expressions $\sigma_\perp^{\text{QFT}}$. This important difference between CM/QM and QFT results manifests itself through an analogy of the anisotropic factor $\frac{1}{1+\frac{\tau_c^2}{\tau_B^2}}$ in the CM/QM sector to the factor $\frac{\Gamma}{(\mu-\sqrt{\mu^2-2eB})^2+\Gamma^2}$ in QFT sector. We have taken the ratio of cyclotron time period for CM/QM to that of QFT $\tau_B/\tilde{\tau}_B$ and plotted against $eB$ and $\mu$ in Figs. 6(a) and 6(b) respectively, where a clear deviation from one is noticed for quantum domain i.e., high $eB$ and low $\mu$ regions. We see that cyclotron time period for CM is larger than that of QFT in that domain. It means that QFT push the system with a larger cyclotron frequency and lesser cyclotron time period, for which the anisotropic conduction will also be increased.

## IV. SUMMARY AND CONCLUSIONS

In the present work have explored the field theoretical structure of the electrical conductivity of degenerate relativistic fermionic matter in presence of magnetic field. With the help of Schwinger's proper-time formalism, two-point function of current-current correlator in the one-loop diagram level is obtained for the degenerate fermionic medium. Owing to the Kubo relation, the conductivity tensor is realized as the zero-momentum limit of the current-current correlator, whose one-loop level diagram carries two propagators with two different Landau level sumations. Due to the orthogonal properties of Laguerre polynomials, the conduction along perpendicular direction selects $\pm 1$ differences of Landau levels of propagators, while parallel conduction selects propagators with same Landau levels. This fact is well established in our earlier work [39] for finite-temperature calculation, which is modified in the present work for the finite density picture relevant for compact star environment.

After going through a rigorous calculation, based on real-time formalism thermal-field theory, we finally get

very simple algebric relations with a Landau level summation. Based on the relaxation-time approximation (RTA) method, Ref. [41] has obtained similar kinds of algebric expressions for degenerate fermionic matter, which is called the classical mechanical (CM) expressions, and its Landau quantization extension is called the quantum mechanical expressions for distinguishing them from our quantum field theoretical expressions, addressed in present work. The background of CM and QM expressions are the RTA-based kinetic theory approach but the background of the QFT expression is the Kubo approach. Their background methods are completely different. However, the interesting news revealed by the present work, is that the QFT expression is exactly same as the QM expression for the parallel conductivity component but they are different for the perpendicular component. It is the nonzero cyclotron frequency which is entered into the CM expression of the perpendicular component of electrical conductivity and is responsible for reducing its conduction along the perpendicular direction with respect to its parallel component. In the QFT expression of perpendicular conductivity, we get a completely new expression of cyclotron frequency, which become much larger than its classical values in the quantum domain. Low chemical potentials and high magnetic fields can be considered as the quantum domain, where the parallel and perpendicular conductivity components get an oscillating pattern like the Shubnikov-de Haas (SdH) oscillation, which is a well-known phenomenon in condensed matter physics. The present work anticipates a possibility of SdH or quantized patterns of conductivity tensor in the compact star environment, which may demand more future works related with this particular topic from theoretical and phenomenological sides of the astrophysics sector.

Finally, let us locate the limitation of our present calculation. We are confined here within the one-loop calculation but for a real system, having the interaction Lagrangian density, infinite-order ladder diagrams [75,76] have to be considered as they all may contribute in same

order of magnitude. Such resummation of the ladder diagrams in the presence of external magnetic fields in the calculation of the longitudinal conductivity of quark matter has been performed using the LLL approximation in Ref. [77] and including all the Landau levels in Ref. [78]. At present, there are no other calculations for the transverse conductivity done in QM and QFT approaches which can support our findings or bring a more clear picture on the issues, like whether QFT is a more mature expression than QM or not; and whether the difference between QFT and QM is sensible or not. Finally, we also note that, in the Kubo approach at nonzero magnetic field, we introduced the finite thermal width $\Gamma$ as a parameter (by hand) instead of calculating it from the interaction Lagrangian. Depending upon the systems, we have to consider the corresponding interaction Lagrangian density and have to calculate $\Gamma$ from it. These all are future scopes for the extension of the present work.

## ACKNOWLEDGMENTS

## APPENDIX A: CALCULATION OF THE TWO-POINT CORRELATION FUNCTION

In this appendix, we will calculate the two-point vector current correlation function $\langle \mathcal{T}_C J^\mu(x) J^\nu(y) \rangle_{11}^B$ in the presence of external magnetic field. We have from Eq. (3)

$$\langle \mathcal{T}_c J^\mu(x) J^\nu(y) \rangle_{11}^B = e^2 \langle \mathcal{T}_c \bar{\psi}(x) \gamma^\mu \psi(x) \bar{\psi}(y) \gamma^\nu \psi(y) \rangle_{11}^B. \tag{A1}$$

Applying Wick's theorem on the right-hand side of Eq. (A1) yields

$$\langle \mathcal{T}_c J^\mu(x) J^\nu(y) \rangle_{11}^B = e^2 \langle \mathcal{T}_C \bar{\psi}(x) \gamma^\mu \psi(x) \bar{\psi}(y) \gamma^\nu \psi(y) \rangle_{11}^B$$
$$= -e^2 \text{Tr}\{\gamma^\mu S_{11}^B(x,y) \gamma^\nu S_{11}^B(y,x)\}, \tag{A2}$$

where, $S_{11}^B(x,y) = \langle \mathcal{T}_C \psi(x) \bar{\psi}(y) \rangle_{11}^B$ denotes the 11-component of the coordinate space thermodense-magnetic Dirac propagator in RTF. It is to be noted that Eq. (A2) remains valid even if the fermion field $\psi$ is a multiplet, in which case, the traces will have to be taken over all the spaces belonging to the multiplet in addition to the Dirac space. The magnetized Dirac propagator $S_{11}^B(x,y) = \Phi(x,y) S_{11}^B(x-y)$ is not translationally invariant due to the gauge-dependent phase factor $\Phi(x,y)$ (which explicitly breaks the translational invariance) however, it can partially be Fourier transformed to the momentum space as

$$S_{11}^B(x,y) = \Phi(x,y) \int \frac{d^4 p}{(2\pi)^4} e^{-ip \cdot (x-y)} (-i S_{11}^B(p)), \tag{A3}$$

where, $S_{11}^B(p)$ is the 11-component of the momentum space-free thermodense-magnetic Dirac propagator in RTF whose explicit form reads [46,79,80]

$$S_{11}^B(p) = \sum_{l=0}^{\infty} (-1)^l e^{-\alpha_p} \mathcal{D}_l(p) D_{11}(p_\parallel, m_l). \tag{A4}$$

In the above equation, $l$ denotes the Landau level index, $\alpha_p = -\frac{p_\perp^2}{eB} \geq 0$, $m_l = \sqrt{m^2 + 2leB}$ is the "Landau level dependent effective mass", $\mathcal{D}_l(p)$ contains the complicated Dirac structure involving the Laguerre polynomials as

$$\mathcal{D}_l(p) = (\not{p}_\parallel + m)[(\mathbb{1} + i\gamma^1\gamma^2)L_l(2\alpha_p)$$
$$- (\mathbb{1} - i\gamma^1\gamma^2)L_{l-1}(2\alpha_p)] - 4\not{p}_\perp L_{l-1}^1(2\alpha_p), \tag{A5}$$

with the convention $L_{-1}(z) = L_{-1}^1(z) = 0$, and $D_{11}(p, m)$ is given by

$$D_{11}(p,m) = \left[ \frac{-1}{p^2 - m^2 + i\epsilon} - \xi(p.u) 2\pi i \delta(p^2 - m^2) \right], \tag{A6}$$

in which $\xi(x) = \Theta(x)f_+(x) + \Theta(-x)f_-(-x)$, $f_\pm(x) = [e^{(x \mp \mu)/T} + 1]^{-1}$ are the Fermi-Dirac thermal distribution functions, and $u^\mu$ is the medium four-velocity. In the local rest frame (LRF) of the medium $u_{\text{LRF}}^\mu \equiv (1, \vec{0})$.

Substituting Eq. (A3) into Eq. (A2), we get

$$\langle \mathcal{T}_C J^\mu(x) J^\nu(y) \rangle_{11}^B$$
$$= e^2 \Phi(x,y) \Phi(y,x) \iint \frac{d^4 p}{(2\pi)^4} \frac{d^4 k}{(2\pi)^4} e^{-i(x-y)\cdot(p-k)}$$
$$\times \text{Tr}\{\gamma^\mu S_{11}^B(p) \gamma^\nu S_{11}^B(k)\}. \tag{A7}$$

Again substituting Eq. (A4) into Eq. (A7) and using the fact that $\Phi(x,y)\Phi(y,x) = 1$, we get (after a bit of simplification)

$$\langle \mathcal{T}_C J^\mu(x) J^\nu(y) \rangle_{11}^B$$
$$= -\sum_{l=0}^{\infty} \sum_{n=0}^{\infty} \iint \frac{d^4 p}{(2\pi)^4} \frac{d^4 k}{(2\pi)^4} e^{-i(x-y)\cdot(p-k)}$$
$$\times D_{11}(p_\parallel, m_n) D_{11}(k_\parallel, m_l) \mathcal{N}_{ln}^{\mu\nu}(k,p), \tag{A8}$$

where

$$\mathcal{N}_{ln}^{\mu\nu}(k,p) = -e^2(-1)^{l+n}e^{-\alpha_k-\alpha_p}\text{Tr}\{\gamma^\mu \mathcal{D}_n(p)\gamma^\nu \mathcal{D}_l(k)\}. \tag{A9}$$

In the calculation of the electrical conductivity, we actually require the expressions of $\mathcal{N}_{ln}^{\mu\nu}(k,k)$ and $\tilde{\mathcal{N}}_{ln}^{\mu\nu}(k_\parallel) = \int \frac{d^2k_\perp}{(2\pi)^2}\mathcal{N}_{ln}^{\mu\nu}(k,k)$. From Eq. (A9), we get (after evaluating the traces over Dirac matrices)

$$\begin{aligned}
\mathcal{N}_{ln}^{\mu\nu}(k,k) = -8e^2[&8(2k_\perp^\mu k_\perp^\nu - k_\perp^2 g^{\mu\nu})\mathcal{B}_{ln}(k_\perp^2) \\
&+ \{2k_\parallel^\mu k_\parallel^\nu - g_\parallel^{\mu\nu}(k_\parallel^2 - m^2)\}\mathcal{C}_{ln}(k_\perp^2) \\
&+ g_\perp^{\mu\nu}(k_\parallel^2 - m^2)\mathcal{D}_{ln}(k_\perp^2) \\
&+ 2(k_\parallel^\nu k_\perp^\mu + k_\parallel^\mu k_\perp^\nu)\mathcal{E}_{ln}(k_\perp^2)],
\end{aligned} \tag{A10}$$

where

$$\mathcal{B}_{ln}(k_\perp^2) = (-1)^{l+n}e^{-2\alpha_k}L_{l-1}^1(2\alpha_k)L_{n-1}^1(2\alpha_k), \tag{A11}$$

$$\begin{aligned}
\mathcal{C}_{ln}(k_\perp^2) = (-1)^{l+n}e^{-2\alpha_k}\{&L_{l-1}(2\alpha_k)L_{n-1}(2\alpha_k) \\
&+ L_l(2\alpha_k)L_n(2\alpha_k)\},
\end{aligned} \tag{A12}$$

$$\begin{aligned}
\mathcal{D}_{ln}(k_\perp^2) = (-1)^{l+n}e^{-2\alpha_k}\{&L_l(2\alpha_k)L_{n-1}(2\alpha_k) \\
&+ L_{l-1}(2\alpha_k)L_n(2\alpha_k)\},
\end{aligned} \tag{A13}$$

$$\begin{aligned}
\mathcal{E}_{ln}(k_\perp^2) = (-1)^{l+n}e^{-2\alpha_k}\{&L_{l-1}(2\alpha_k)L_{n-1}^1(2\alpha_k) \\
&- L_l(2\alpha_k)L_{n-1}^1(2\alpha_k). \\
&+ L_{l-1}^1(2\alpha_k)L_{n-1}(2\alpha_k) \\
&- L_{l-1}^1(2\alpha_k)L_n(2\alpha_k)\}.
\end{aligned} \tag{A14}$$

Using Eq. (A10), we obtain

$$\begin{aligned}
\tilde{\mathcal{N}}_{ln}^{\mu\nu}(k_\parallel) &= \int \frac{d^2k_\perp}{(2\pi)^2}\mathcal{N}_{ln}^{\mu\nu}(k,k) \\
&= 8e^2[8\mathcal{B}_{ln}^{(2)}g^{\mu\nu} - \mathcal{C}_{ln}^{(0)}\{2k_\parallel^\mu k_\parallel^\nu - g_\parallel^{\mu\nu}(k_\parallel^2 - m^2)\} \\
&\quad - \mathcal{D}_{ln}^{(0)}(k_\parallel^2 - m^2)g_\perp^{\mu\nu}],
\end{aligned} \tag{A15}$$

where

$$\mathcal{B}_{ln}^{(j)} = \int \frac{d^2k_\perp}{(2\pi)^2}\mathcal{B}_{ln}(k_\perp^2)(k_\perp^2)^{j/2}, \tag{A16}$$

$$\mathcal{C}_{ln}^{(j)} = \int \frac{d^2k_\perp}{(2\pi)^2}\mathcal{C}_{ln}(k_\perp^2)(k_\perp^2)^{j/2}, \tag{A17}$$

$$\mathcal{D}_{ln}^{(j)} = \int \frac{d^2k_\perp}{(2\pi)^2}\mathcal{D}_{ln}(k_\perp^2)(k_\perp^2)^{j/2}. \tag{A18}$$

Exploiting the orthogonality of the Laguerre polynomials present in the functions $\mathcal{B}_{ln}(k_\perp^2)$, $\mathcal{C}_{ln}(k_\perp^2)$, and, $\mathcal{D}_{ln}(k_\perp^2)$, the $d^2k_\perp$ integrals of Eqs. (A16)–(A18) are performed and the analytic expressions of the quantities $\mathcal{B}_{ln}^{(j)}$, $\mathcal{C}_{ln}^{(j)}$, and, $\mathcal{D}_{ln}^{(j)}$ are provided in Appendix B. On substituting Eqs. (B3)–(B5) into Eq. (A15), we finally arrive at

$$\begin{aligned}
\tilde{\mathcal{N}}_{ln}^{\mu\nu}(k_\parallel) &= \int \frac{d^2k_\perp}{(2\pi)^2}\mathcal{N}_{ln}^{\mu\nu}(k,k) \\
&= e^2\frac{eB}{\pi}[-4eBn\delta_{l-1}^{n-1}g_\parallel^{\mu\nu} \\
&\quad - (\delta_l^n + \delta_{l-1}^{n-1})\{2k_\parallel^\mu k_\parallel^\nu - g_\parallel^{\mu\nu}(k_\parallel^2 - m^2)\} \\
&\quad + (\delta_l^{n-1} + \delta_{l-1}^n)(k_\parallel^2 - m^2)g_\perp^{\mu\nu}].
\end{aligned} \tag{A19}$$

## APPENDIX B: ANALYTIC EXPRESSIONS OF $\mathcal{B}_{ln}^{(j)}$, $\mathcal{C}_{ln}^{(j)}$, AND, $\mathcal{D}_{ln}^{(j)}$

Using the orthogonality of the Laguerre polynomials, the following integral identities can be derived

$$\int \frac{d^2k_\perp}{(2\pi)^2}e^{-2\alpha_k}L_{l-1}^1(2\alpha_k)L_{n-1}^1(2\alpha_k)k_\perp^2 = -\frac{(eB)^2}{16\pi}n\delta_{l-1}^{n-1}, \tag{B1}$$

$$\int \frac{d^2k_\perp}{(2\pi)^2}e^{-2\alpha_k}L_l(2\alpha_k)L_n(2\alpha_k) = \frac{eB}{8\pi}\delta_l^n. \tag{B2}$$

Using Eqs. (B1) and (B1), we now perform the $d^2k_\perp$ integrals of Eqs. (A16)–(A18) and obtain

$$\mathcal{B}_{ln}^{(2)} = -\frac{(eB)^2}{16\pi}n\delta_{l-1}^{n-1}, \tag{B3}$$

$$\mathcal{C}_{ln}^{(0)} = \frac{eB}{8\pi}(\delta_l^n + \delta_{l-1}^{n-1}), \tag{B4}$$

$$\mathcal{D}_{ln}^{(0)} = -\frac{eB}{8\pi}(\delta_l^{n-1} + \delta_{l-1}^n). \tag{B5}$$

It is to be noted that, the Kronecker delta function having a negative index is always zero (i.e., $\delta_{-1}^{-1} = 0$). This is due to restrictions on the Laguerre polynomials $L_{-1}(z) = L_{-1}^1(z) = 0$ used in defining the magnetized Dirac propagator in Eq. (A6).

[1] A. K. Harding and D. Lai, Rep. Prog. Phys. **69,** 2631 (2006).
[2] J. H. Seiradakis and R. Wielebinski, Astron. Astrophys. Rev. **12,** 239 (2004).
[3] http://www.physics.mcgill.ca/pulsar/magnetar/main.html.
[4] S. L. Shapiro and S. A. Teukolsky, *Black Holes, White Dwarfs, and Neutron Stars: The Physics of Compact Objects* (Wiley, New York, USA, 1983), 10.1002/asna.2113050518.
[5] E. Annala, T. Gorda, A. Kurkela, J. Nättilä, and A. Vuorinen, Nat. Phys. **16,** 907 (2020).
[6] D. E. Kharzeev, K. Landsteiner, A. Schmitt, and H.-U. Yee, Lect. Notes Phys. **871,** 1 (2013).
[7] P. Goldreich and A. Reisenegger, Astrophys. J. **395,** 250 (1992).
[8] K. Dionysopoulou, D. Alic, C. Palenzuela, L. Rezzolla, and B. Giacomazzo, Phys. Rev. D **88,** 044020 (2013).
[9] C. Palenzuela, L. Lehner, M. Ponce, S. L. Liebling, M. Anderson, D. Neilsen, and P. Motl, Phys. Rev. Lett. **111,** 061105 (2013).
[10] C. Palenzuela, L. Lehner, S. L. Liebling, M. Ponce, M. Anderson, D. Neilsen, and P. Motl, Phys. Rev. D **88,** 043011 (2013).
[11] K. Dionysopoulou, D. Alic, and L. Rezzolla, Phys. Rev. D **92,** 084064 (2015).
[12] A. Harutyunyan, A. Nathanail, L. Rezzolla, and A. Sedrakian, Eur. Phys. J. A **54,** 191 (2018).
[13] B. P. Abbott *et al.* (LIGO Scientific, Virgo Collaborations), Phys. Rev. Lett. **119,** 161101 (2017).
[14] L. Mestel, Math. Proc. Cambridge Philos. Soc. **46,** 331 (1950).
[15] A. A. Abrikosov, Sov. Phys. JETP **18,** 1399 (1964), http://jetp.ras.ru/cgi-bin/e/index/e/18/5/p1399?a=list.
[16] V. Canuto, Astrophys. J. **159,** 641 (1970).
[17] E. Flowers and N. Itoh, Astrophys. J. **206,** 218 (1976).
[18] V. Canuto and H. Y. Chiu, Phys. Rev. **188,** 2446 (1969).
[19] V. Canuto and C. Chiuderi, Phys. Rev. D **1,** 2219 (1970).
[20] A. Y. Potekhin, Astron. Astrophys. **351,** 787 (1999), https://ui.adsabs.harvard.edu/abs/1999A%26A...351..787P/abstract.
[21] E. Østgaard and D. G. Yakovlev, Nucl. Phys. **A540,** 211 (1992).
[22] B. O. Kerbikov and M. A. Andreichikov, Phys. Rev. D **91,** 074010 (2015).
[23] D. A. Baiko, Mon. Not. R. Astron. Soc. **458,** 2840 (2016).
[24] A. Harutyunyan and A. Sedrakian, Phys. Rev. C **94,** 025805 (2016).
[25] S.-i. Nam, Phys. Rev. D **86,** 033014 (2012).
[26] K. Hattori, S. Li, D. Satow, and H.-U. Yee, Phys. Rev. D **95,** 076008 (2017).
[27] M. Kurian, S. Mitra, S. Ghosh, and V. Chandra, Eur. Phys. J. C **79,** 134 (2019).
[28] M. Kurian and V. Chandra, Phys. Rev. D **96,** 114026 (2017).
[29] B. Feng, Phys. Rev. D **96,** 036009 (2017).
[30] K. Fukushima and Y. Hidaka, Phys. Rev. Lett. **120,** 162301 (2018).
[31] A. Das, H. Mishra, and R. K. Mohapatra, Phys. Rev. D **101,** 034027 (2020).
[32] A. Das, H. Mishra, and R. K. Mohapatra, Phys. Rev. D **100,** 114004 (2019).
[33] A. Das, H. Mishra, and R. K. Mohapatra, Phys. Rev. D **99,** 094031 (2019).
[34] J. Dey, S. Satapathy, P. Murmu, and S. Ghosh, Pramana **95,** 125 (2021).
[35] J. Dey, S. Satapathy, A. Mishra, S. Paul, and S. Ghosh, Int. J. Mod. Phys. E **30,** 2150044 (2021).
[36] A. Dash, S. Samanta, J. Dey, U. Gangopadhyaya, S. Ghosh, and V. Roy, Phys. Rev. D **102,** 016016 (2020).
[37] S. Ghosh, A. Bandyopadhyay, R. L. S. Farias, J. Dey, and G. a. Krein, Phys. Rev. D **102,** 114015 (2020).
[38] S. Samanta, J. Dey, S. Satapathy, and S. Ghosh, arXiv:2002.04434.
[39] S. Satapathy, S. Ghosh, and S. Ghosh, Phys. Rev. D **104,** 056030 (2021).
[40] G. Baym, T. Hatsuda, T. Kojo, P. D. Powell, Y. Song, and T. Takatsuka, Rep. Prog. Phys. **81,** 056902 (2018).
[41] J. Dey, A. Bandyopadhyay, A. Gupta, N. Pujari, and S. Ghosh, arXiv:2103.15364.
[42] L. Schubnikow and W. De Haas, Proc. R. Neth. Acad. Arts Sci. **33,** 130 (1930).
[43] L. Schubnikow and W. De Haas, Proc. R. Neth. Acad. Arts Sci. **33,** 363 (1930).
[44] L. Schubnikow and W. De Haas, Proc. R. Neth. Acad. Arts Sci. **33,** 418 (1930).
[45] L. Schubnikow and W. De Haas, Proc. R. Neth. Acad. Arts Sci. **33,** 433 (1930).
[46] J. S. Schwinger, Phys. Rev. **82,** 664 (1951).
[47] T.-K. Chyi, C.-W. Hwang, W. F. Kao, G.-L. Lin, K.-W. Ng, and J.-J. Tseng, Phys. Rev. D **62,** 105014 (2000).
[48] A. Kuznetsov and N. Mikheev, Springer Tracts Mod. Phys. **197,** 1 (2004).
[49] *Electroweak Processes in External Active Media*, edited by A. Kuznetsov and N. Mikheev, Springer Tracts in Modern Physics (Springer, Heidelberg, Germany, 2013), Vol. 252, 10.1007/978-3-642-36226-2.
[50] M. D. Schwartz, *Quantum Field Theory and the Standard Model* (Cambridge University Press, Cambridge, England, 2014).
[51] E. A. Calzetta and B.-L. B. Hu, *Nonequilibrium Quantum Field Theory*, Cambridge Monographs on Mathematical Physics (Cambridge University Press, Cambridge, England, 2008).
[52] D. J. Toms, *The Schwinger Action Principle and Effective Action*, Cambridge Monographs on Mathematical Physics (Cambridge University Press, Cambridge, England, 2012).
[53] T. Inagaki, D. Kimura, and T. Murata, Int. J. Mod. Phys. A **20,** 4995 (2005).
[54] A. V. Kuznetsov, A. A. Okrugin, and A. M. Shitova, Int. J. Mod. Phys. A **30,** 1550140 (2015).
[55] A. Ayala, A. Sanchez, G. Piccinelli, and S. Sahu, Phys. Rev. D **71,** 023004 (2005).
[56] M. L. Bellac, *Thermal Field Theory*, Cambridge Monographs on Mathematical Physics (Cambridge University Press, Cambridge, England, 2011).
[57] S. Mallik and S. Sarkar, *Hadrons at Finite Temperature* (Cambridge University Press, Cambridge, England, 2016).
[58] J. Kapusta and C. Gale, *Finite-Temperature Field Theory: Principles and Applications*, Cambridge Monographs on

Mathematical Physics (Cambridge University Press, Cambridge, England, 2011).

[59] S. Mallik and S. Sarkar, Eur. Phys. J. C **61**, 489 (2009).

[60] H. A. Weldon, Phys. Rev. D **76**, 125029 (2007).

[61] R. L. Kobes, G. W. Semenoff, and N. Weiss, Z. Phys. C **29**, 371 (1985).

[62] T. Lundberg and R. Pasechnik, Eur. Phys. J. A **57**, 71 (2021).

[63] D. N. Zubarev, *Nonequilibrium Statistical Thermodynamics* (Consultants Bureau, New York, 1974).

[64] D. N. Zubarev, V. Morozov, and G. Ropke, *Statistical Mechanics of Nonequilibrium Processes, Volume 1: Basic Concepts, Kinetic Theory* (Akademie Verlag GmbH, Berlin, 1996).

[65] X.-G. Huang, A. Sedrakian, and D. H. Rischke, Ann. Phys. (Amsterdam) **326**, 3075 (2011).

[66] A. Hosoya, M.-a. Sakagami, and M. Takao, Ann. Phys. (N.Y.) **154**, 229 (1984).

[67] S. Ghosh, G. a. Krein, and S. Sarkar, Phys. Rev. C **89**, 045201 (2014).

[68] U. Gangopadhyaya, S. Ghosh, S. Sarkar, and S. Mitra, Phys. Rev. C **94**, 044914 (2016).

[69] M. Rahaman, S. Ghosh, S. Ghosh, S. Sarkar, and J.-e. Alam, Phys. Rev. C **97**, 035201 (2018).

[70] S. Ghosh, S. Mitra, and S. Sarkar, Nucl. Phys. **A969**, 237 (2018).

[71] S. Ghosh, S. Ghosh, and S. Bhattacharyya, Phys. Rev. C **98**, 045202 (2018).

[72] S. Ghosh and V. Chandra, Eur. Phys. J. A **56**, 190 (2020).

[73] P. Elmfors, D. Persson, and B.-S. Skagerstam, Astropart. Phys. **2**, 299 (1994).

[74] P. Elmfors, D. Persson, and B.-S. Skagerstam, Phys. Rev. Lett. **71**, 480 (1993).

[75] S. Jeon, Phys. Rev. D **52**, 3591 (1995).

[76] D. Fernandez-Fraile and A. Gomez Nicola, Phys. Rev. D **73**, 045025 (2006).

[77] K. Hattori and D. Satow, Phys. Rev. D **94**, 114032 (2016).

[78] K. Fukushima and Y. Hidaka, J. High Energy Phys. 04 (2020) 162.

[79] A. Ayala, A. Bashir, and S. Sahu, Phys. Rev. D **69**, 045008 (2004).

[80] A. Mukherjee, S. Ghosh, M. Mandal, P. Roy, and S. Sarkar, Phys. Rev. D **96**, 016024 (2017).